Received: 11 September 2021 | Revised: 31 December 2021 | Accepted: 9 February 2022

DOI: 10.1002/ijc.33983

CANCER GENETICS AND EPIGENETICS

IJC INTERNATIONAL JOURNAL of CANCER

Integrated molecular profiling of patient-derived ovarian cancer models identifies clinically relevant signatures and tumor vulnerabilities

Michela Lupia[1] | Valentina Melocchi[2] | Francesca Bizzaro[3] | Pietro Lo Riso[4] | Elisa Dama[2] | Micol Baronio[1] | Alberto Ranghiero[5] | Massimo Barberis[5] | Loris Bernard[6] | Giovanni Bertalot[4] | Raffaella Giavazzi[3] | Giuseppe Testa[4,7] | Fabrizio Bianchi[2] | Ugo Cavallaro[1]

[1]Unit of Gynaecological Oncology Research, European Institute of Oncology IRCCS, Milan, Italy

[2]Unit of Cancer Biomarkers, Fondazione IRCCS Casa Sollievo della Sofferenza, San Giovanni Rotondo, Italy

[3]Laboratory of Tumor Metastasis Therapeutics, Istituto di Ricerche Farmacologiche Mario Negri-IRCCS, Milan, Italy

[4]Department of Experimental Oncology, European Institute of Oncology IRCCS, Milan, Italy

[5]Pathology Unit, European Institute of Oncology IRCCS, Milan, Italy

[6]Clinical Genomics Lab, European Institute of Oncology IRCCS, Milan, Italy

[7]Department of Oncology and Haemato-Oncology, University of Milan, Italy

Correspondence
Ugo Cavallaro, Unit of Gynaecological Oncology Research, European Institute of Oncology IRCSS, Via Adamello 16, 20139 Milano, Italy.
Email: ugo.cavallaro@ieo.it

Fabrizio Bianchi, Unit of Cancer Biomarkers, Fondazione IRCCS Casa Sollievo della Sofferenza, Viale Padre Pio, 7, 71013 San Giovanni Rotondo (FG), Italy.
Email: f.bianchi@operapadrepio.it

Abstract

High-grade serous ovarian carcinoma (HGSOC) is a highly aggressive and intractable neoplasm, mainly because of its rapid dissemination into the abdominal cavity, a process that is favored by tumor-associated peritoneal ascites. The precise molecular alterations involved in HGSOC onset and progression remain largely unknown due to the high biological and genetic heterogeneity of this tumor. We established a set of different tumor samples (termed the As11-set) derived from a single HGSOC patient, consisting of peritoneal ascites, primary tumor cells, ovarian cancer stem cells (OCSC) and serially propagated tumor xenografts. The As11-set was subjected to an integrated RNA-seq and DNA-seq analysis which unveiled molecular alterations that marked the different types of samples. Our profiling strategy yielded a panel of signatures relevant in HGSOC and in OCSC biology. When such signatures were used to interrogate the TCGA dataset from HGSOC patients, they exhibited prognostic and predictive power. The molecular alterations also identified potential vulnerabilities associated with OCSC, which were then tested functionally in stemness-related assays. As a proof of concept, we defined PI3K signaling as a novel druggable target in OCSC.

KEYWORDS
ascites, cancer stem cells, genomics, ovarian cancer, prognosis, xenograft

Abbreviations: CL, late-passage As11 cell line; CNV, copy number variation; EMT, epithelial-mesenchymal transition; EOC, epithelial ovarian cancer; GO, gene ontology; HGSOC, high-grade serous ovarian cancer; MCP, microenvironment cell populations; OCSC, ovarian cancer stem cells; PDX, patient-derived xenograft; PI3K, phosphoinositide 3-kinase; PIK3CA, phosphoinositide 3-kinase catalytic subunit alpha; PIK3R1, phosphoinositide 3-kinase regulatory subunit 1; PR, early-passage primary As11 cells; QT, quantitative trait.

Michela Lupia and Valentina Melocchi shared equally to the first authorship and Fabrizio Bianchi and Ugo Cavallaro shared equally to the last authorship.

Present address
Giovanni Bertalot, Division of Anatomical Pathology, Santa Chiara Hospital, Trento, Italy

Funding information
Associazione Italiana per la Ricerca sul Cancro, Grant/Award Numbers: IG-14622, IG-2017, IG-21320, IG-22827, IG-23250, MFAG-17568; Fondazione Istituto Europeo di Oncologia-Centro Cardiologico Monzino; Ministero della Salute, Grant/Award Numbers: GR-2016-02363975, RF-2016-02362551; Roche per la Ricerca; Fondazione Italiana per la Ricerca sul Cancro; Fondazione Umberto Veronesi; Ministry of Health

What's new?

High-grade serous ovarian carcinoma (HGSOC) is aggressive and frequently fatal, and its high degree of heterogeneity has made it difficult to characterize the molecular changes that promote its progression. Here, the authors collected a set of samples from a single patient consisting of multiple cell types representing different steps in tumor progression. They conducted DNA and RNA sequencing to create a panel of molecular signatures that distinguished the different cell types. This panel not only showed prognostic value, it also revealed the PI3K signaling pathway as a potential druggable target in ovarian cancer stem cells.

1 | INTRODUCTION

Epithelial ovarian cancer (EOC) is the most lethal gynecological tumor in developed countries.[1] Among the various EOC histotypes, high-grade serous EOC (HGSOC) is the most frequent (~70%) and intractable form of the disease.[2] In about 80% of cases, HGSOC is diagnosed at late stage due to the absence of specific symptoms at earlier stages. Overall, the prognosis of patients with HGSOC is dismal, with a survival rate of 30% at 5 years.[3]

Recent efforts have tried to build the evolutionary trajectories of EOC by performing whole-genome sequencing of primary tumors and also of matched metastatic lesions[4,5] in order to track the molecular alterations associated with the metastatic spread of EOC, which represents a major cause of lethality. However, the identification of cancer-driver molecular alterations involved in EOC progression remains an unmet need. Several large-scale studies using next-generation sequencing have investigated the mutational profile of HGSOC. This revealed a high mutational burden, a remarkable intertumor and intratumor genetic heterogeneity and the presence of molecular subtypes,[6,7] which complicates significantly the identification of driver mutations. As an alternative, the molecular profiling of malignant ascites which develops frequently in HGSOC patients and contains metastatic EOC cells,[8] can provide important insights regarding the biology of metastatic HGSOC,[9] the clonal evolution of tumor cells[10] and the identification of biomarkers to guide therapeutic strategies and monitor treatment response.[11]

Malignant ascites contain free-floating multicellular tumor aggregates that are enriched in ovarian cancer stem cells (OCSCs) which, in turn, drive tumor formation, dissemination and recurrence, as well as drug resistance.[12] We recently showed that it was possible to unveil mechanisms, particularly relevant in tumor initiation and stemness of HGSOC by coupling the analysis of OCSC-enriched spheroids to that of matched primary tumor samples.[13]

Our study provides a comprehensive investigation of the molecular alterations occurring in HGSOC ascites-derived metastatic cancer cells and OCSCs. The ascites from a HGSOC patient was utilized to derive matched tumor samples (primary cells, OCSC-enriched spheroids, serially propagated patient-derived xenografts) that could recapitulate key steps of tumor progression, such as initiation, metastatic outgrowth and stemness. Through an integrated genomic and transcriptomic analysis, we dissected the molecular alterations that mark the different types of samples, which allowed to identify signatures associated with HGSOC progression. The prognostic value of such signatures and the definition of PI3K signaling as a novel vulnerability in OCSCs indicated that our approach can provide clinically relevant insights, including the possible identification of druggable targets in HGSOC ascites, which are major responsible for relapse disease and poor prognosis.

2 | MATERIALS AND METHODS

2.1 | Isolation, culture and processing of primary epithelial ovarian cancer cells

Informed consent was obtained from the patients in the study. Our study was performed in accordance with the Declaration of Helsinki and was approved by the European Institute of Oncology Ethics Committee (protocol no. R789-IEO). Peritoneal ascites were collected through paracentesis upon informed consent from a 59-years-old patient of the Gynecology Division of the European Institute of Oncology (Milan) who presented with ovarian masses and other pelvic lesions. The ascites were collected prior to any surgical or pharmacological treatment. The clinical evaluation and the histological analysis of peritoneal biopsies indicated a diagnosis of FIGO Stage-IIIC HGSOC. The isolation and culture of primary cells were performed as previously described.[14] Briefly, immediately after paracentesis, the ascitic fluid was centrifuged to obtain a pellet containing cell aggregates and single cells. Red blood cells were eliminated by two 5-minute treatments with ACK (Ack Cell Lysing Buffer, Lonza) at room temperature. The purity of the primary cell culture was examined by immunostaining for the epithelial cytokeratins 5, 7 and 8, or for pan-cytokeratin and was consistently over 95%. During culture, primary cells underwent spontaneous in vitro immortalization, and a stable cell line could be established. The As11 cell line has currently reached more than 80 passages. Both primary early-passage cancer cells and the cell line were cultured on collagen I-coated plates (Collagen Cellware, Biocoat, Corning) at 37°C in a humidified incubator with 5% CO_2. For cell line authentication, a short-tandem repeat (STR) profile was

generated from the original patient's ascites and compared to the profile of early and late-passage cells (Table S1 and Figure S1). The STR profiling analysis was performed within the last 3 years. The cell line was routinely tested for mycoplasma and all experiments were performed with mycoplasma-free cells. Primary early-passage cells were used at p2 or p3, while the As11 cell line was used between p25 and p30.

2.2 | Spheroid formation assay

The spheroid formation assay was performed as previously described.[13] The spheroid-forming efficiency was defined as the ratio between number of spheroids and number of cells seeded. To perform the whole-exome sequencing and the mRNA sequencing, first-generation spheroids were dissociated and re-seeded as described above to obtain second-generation spheroids. When needed, the PI3K chemical inhibitors LY294002 (Cell Signaling Technology, Danvers, MA), Alpelisib (BYL-719; Selleckchem, Houston, TX) or Copanlisib (BAY 80-6946; Selleckchem) were added at the indicated concentrations to suspension cultures on days 0, 2 and 4 after seeding. Spheroid formation was assessed 7 days after seeding. See also Supporting Information for further information.

2.3 | Cell proliferation assay

Ascites-derived HGSOC primary cells were seeded in quadruplicate on 96-well plates at 5×10^3 cells/well. After 24 hours, primary cells were treated for 3 days with 20 or 50 μM LY294002. Viable cells were counted using the CCK-8 assay following the manufacturer's instructions.

2.4 | Immunofluorescence

Cells were grown on collagen I-coated glass coverslips. Fresh ascites-derived aggregates were cyto-spinned onto microscope slides. Cells were fixed with 4% PFA for 10 minutes at room temperature, followed by immunofluorescence staining with the following antibodies. A list of antibodies used can be found in Supporting Information.

2.5 | Cell lysis and immunoblotting

Early-passage primary As11 cells were cultured under serum-free conditions for 24 hours. Cells were then stimulated for 30 minutes with 10% fetal bovine serum either in the absence or in the presence of 20 or 50 μM LY294002 (PI3K inhibitor). Cells were lysed in RIPA buffer (0.1% SDS, 0.5% sodium deoxycholate, 1% TritonX-100, 150 mM NaCl, 50 mM Tris pH 7.4, 1 mM Na-Orthovanadate, 10 mM NaF and 200X Protease Inhibitor Cocktail from Calbiochem). Lysates were centrifuged and the pellets were discarded. Equal amounts of proteins were separated by SDS-PAGE and transferred onto nitrocellulose membranes.

2.6 | Histopathological analysis

The morphology of patient's tumor tissues was compared to their corresponding xenografts using paraffin-embedded sections. All samples were fixed in 4% PFA and paraffin-embedded.

The histopathological evaluation of tumor tissues and xenografts was performed by a board-certified pathologist (GB). See also Supporting Information for further information.

2.7 | Animals

Female severe combined immunodeficiency (SCID) and NCr-nu/nu (nude) mice were obtained from Envigo Laboratories (Correzzana, Italy) were used when 6 to 8 weeks old. Mice were maintained under specific pathogen-free conditions, housed in isolated vented cages and handled using aseptic procedures. Procedures involving animals and their care were conducted in conformity with institutional guidelines at the IRCCS-Istituto di Ricerche Farmacologiche Mario Negri, in compliance with the protocol of the Italian Ministry of Health (as required by the Italian Law; protocol no. 945/2016-PR) and in accordance with EU directive 2010/63.

2.8 | Ovarian carcinoma xenograft

Ascites-derived tumor cell aggregates were engrafted in SCID and then propagated in nude mice within 24 hours of collection by serial intraperitoneal (i.p.) transplantation as tumor suspension. Briefly, ascites were centrifuged, the pellet was resuspended in HBSS and injected i.p into nude mice at a dose of 10-20 $\times$ 10^6 cells per mouse. All mice were inspected daily to evaluate tumor growth as the presence of abdominal distension (due to ascites) and palpable tumor masses in the peritoneal cavity.[15,16] Mice were sacrificed when they presented signs of discomfort (reduced mobility and activity, weight loss, etc.). The mean survival time of tumor-bearing mice was 44 days. At sacrifice, ascites were harvested and the volume recorded. Ascites were then centrifuged and the pellet of tumor cells was washed, resuspended in HBSS and used for serial transplantation into recipient mice. The procedure was repeated four times (ie, PDX#1-4), and the tumor cells harvested from the four PDX generations were used for the analysis.

2.9 | DNA and RNA sequencing

DNA and total RNA were isolated using the AllPrep DNA/RNA Mini Kit (Qiagen) according to manufacturer's protocol and quantified using the 2100 Bioanalyzer (Agilent). TruSeq mRNA kit and Illumina

HiSeq2000 were used for RNA sequencing following the manufacturer's instructions. See also Supporting Information for further information.

The sequencing coverage and quality statistics for each sample are summarized in Table S2.

2.10 | Survival analysis

Overall survival and disease-free survival were defined as the time from the date of tumor resection until death from any cause and new tumor event, respectively. Survival was represented by Kaplan-Meier curves and the log-rank test was used to assess the significance of differences in survival experience. Cox regression model was employed to assess simultaneous effects on survival. A nested likelihood ratio test was used to compare models. Platinum status was defined as in Verhaak et al,[17] that is, patients were "RESISTANT" if having tumor recurrence within 6 months after the end of platinum therapy, otherwise were considered as "SENSITIVE." Patients with unknown platinum status (N = 158) were excluded from analysis. Unconditional logistic regression was used to model the odds of resistance as function of QT class. All tests were two sided. *P* values less than .05 were considered statistically significant. Statistical analyses and survival plots were performed using JMP 13 software (SAS).

3 | RESULTS

3.1 | Generation of a set of samples from a HGSOC case

Peritoneal ascites were collected from a 59-years-old HGSOC patient prior to any surgical or pharmacological treatment. The ascites were then processed to isolate fresh tumor aggregates and then establish a primary cell culture, as previously described.[14] Primary HGSOC cells were termed As11, and their origin from HGSOC was confirmed by immunostaining for established markers including CA125, EpCAM and cytokeratins 7 and 8 (Figure 1A) and also specific ovarian cancer markers such as Pax8 and WT1 (Figure S2). To enrich for OCSCs, early-passage primary As11 cells (hereinafter, PR) were cultured in ultra-low attachment plates at low density. Under these conditions, the OCSC subpopulation was able to overcome *anoikis* and proliferate generating monoclonal spheroids (Figure 1B). We have previously demonstrated in several primary cultures of HGSOC (including As11) that, unlike the adherent parental cells, spheroid-forming cells are endowed with stem-like functional properties and express stemness-associated genes (Ref. 13; see also Figure S2B), thus confirming the enrichment in OCSC. In the case of As11, the fraction of spheroid-forming cells in early-passage cultures was approximately 0.4%.[13]

We also observed that with passaging As11 cells underwent spontaneous immortalization. This enabled us to establish a long-term HGSOC cell line (hereinafter, CL) which, incidentally, provides a novel and useful tool for ovarian cancer research. Of note, no significant difference in the expression of OC-associated markers was observed between PR and CL (Figures 1A and S2A), suggesting that CL retains the phenotypical traits of the original HGSOC. So far, the As11 cell line has been passaged more than 80 times in culture.

In parallel to the isolation and culture of primary cells, tumor cell aggregates freshly derived from the patient's ascites (hereinafter, AS) were injected intraperitoneally in immunodeficient mice to generate patient-derived xenografts (PDXs). This resulted in peritoneal dissemination that recapitulated the metastatic sites of human HGSOC (omentum, diaphragm, liver) and in the formation of ascites, in agreement with previous results.[16] In addition, mouse lesions recapitulated the histopathological traits of the patient's tumor (Figure 1C). In particular, both PDXs and the original tumor exhibited glandular neoplastic structures with a large lumen in which papillary projections and necrotic cellular debris were observed. These glandular structures were separated by vascularized connective tissue and occasionally infiltrated by inflammatory cells (Figure 1C). As11-PDXs were serially propagated in mice for up to four passages. Thus, the series of As11 samples (ie, As11-set) that were used for the subsequent molecular profile analyses included the original AS, PR, OCSC, CL and serially propagated orthotopic PDXs.

3.2 | Gene expression analysis of As11-set reveals three distinct gene modules which recapitulate HGSOC transcriptional program

Next, we leveraged the AS11-set to investigate transcriptional patterns representative of biological states relevant for tumor maintenance (ascites and primary tumor cells), stemness (OCSCs) and propagation (PDXs; Section 2). We performed RNA-seq analysis to characterize the whole-transcriptome of As11-set and analyzed 22 341 unique genes in total. Using normalized gene counts, we ran Quantitative Trait (QT) analysis, implemented in the BRB ArrayTools software package[18] (Figure 2A; Section 2), to identify gene expression patterns (ie, QT) which correlate with a set of a priori defined biological states namely "traits" (Section 2; Figure 2B). Since QT analysis does not rely on sample group analysis but it rather measures the correlation of gene expression profile with a "trait" across several experimental conditions (7 in our case), using such an approach we faced the problem of single sample analysis and identified three major significant QTs, that is, (i) QT-A, genes putatively involved in HGSOC initiation whose expression is increased in the serially propagated PDXs and in OCSCs (which have tumor-initiating capability) as compared to the other samples; (ii) QT-B, genes putatively involved in tumor-host interaction and dissemination with high expression in malignant ascites, that is, highly inflammatory environment,[19,20] low in PR and in CL cells (where no host component is present) and increased in propagated PDX samples; (iii) QT-C, genes putatively involved in OCSCs, that is, genes that exhibit moderate expression in malignant ascites and PR and are overexpressed in OCSCs (Figure 2B).

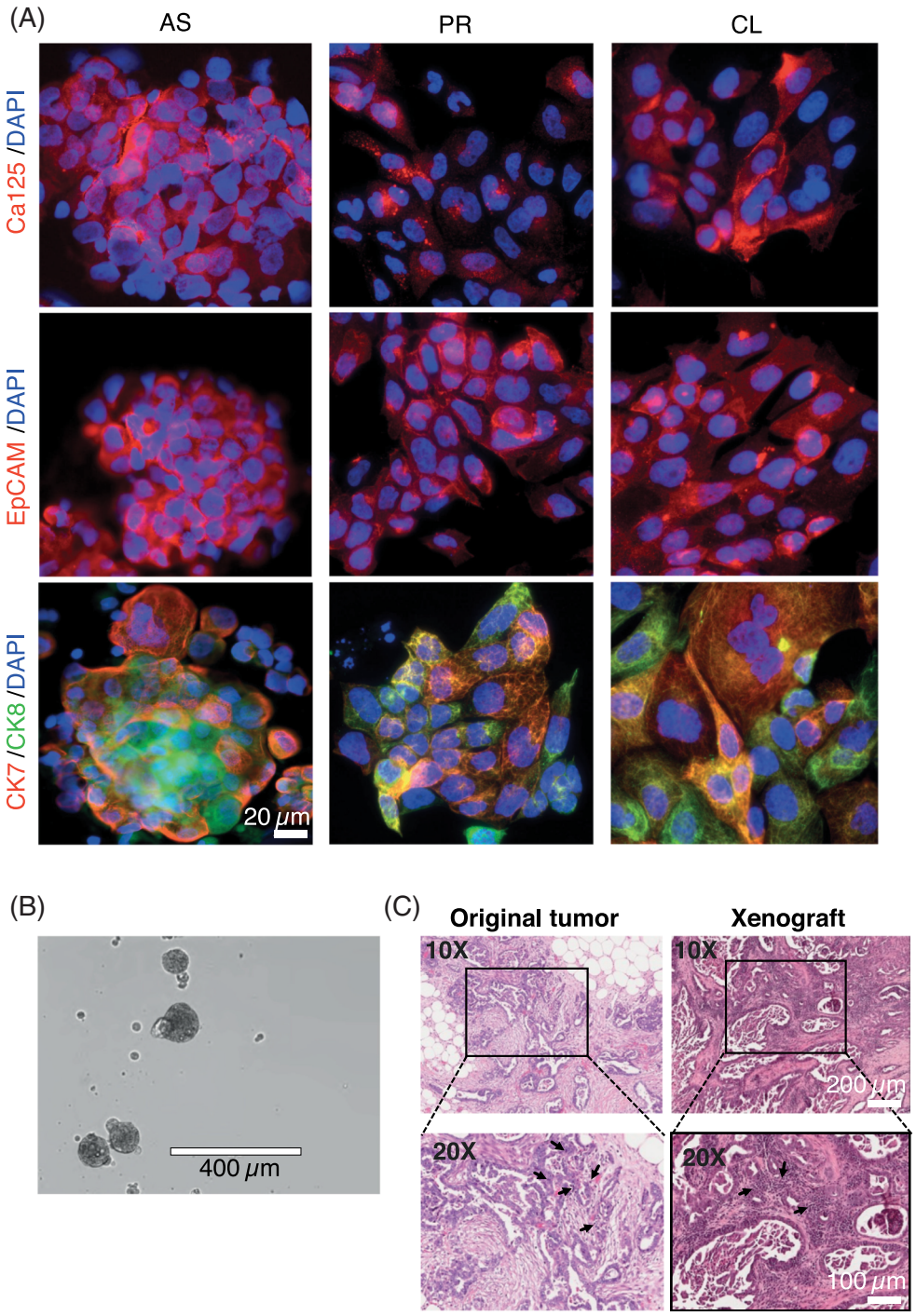

FIGURE 1 Characterization of the As11-set.
(A) Immunophenotypical characterization of As11 primary cells and the spontaneously immortalized cell line. Immunofluorescence staining for the HGSOC markers CA125, EpCAM, CK7 and CK8 was performed on freshly isolated ascites aggregates (AS), primary cells (PR) at early passage (p3) and the established cell line (CL). Nuclei were counterstained with DAPI. Scale bar, 20 μm. (B) Monoclonal spheroids from early-passage primary As11 cells (PR). Scale bar, 400 μm. (C) Hematoxylin/eosin staining of the original As11 tumor (left panel) and the corresponding patient-derived xenograft (right panel). The xenograft showed histopathological features of HGSOC highly similar to the original tumor. The arrows indicate tumor-infiltrating immune cells. Scale bar is as per the legend (100 and 200 μm)

QT analysis scored a total of 819 genes in QT-A ($\rho > 0.8$, $P < .05$), 79 genes in QT-B ($\rho > 0.8$, $P < .05$) and 1425 genes in QT-C ($\rho > 0.8$, $P < .05$; Table S3). QT-C genes were more expressed in PR than CL (Figure 2B). In this regard, a subset of stem-cell/EMT markers belonging to QT-C (CD44, NT5E/CD73 and vimentin) were also validated by immunofluorescence and confirmed an increased fraction of PR expressing these markers (Figure S3A).

Yet, to investigate the biological significance of the identified QTs and exclude possible technical bias due to different environmental conditions characterizing the As11-set sample (ie, human peritoneal cavity, in vitro cell culture and mouse xenograft), we analyzed both gene composition and functions of QT-A, QT-B and QT-C (Table S3) by querying the Molecular Signature Database (MSigDB) and looked at the overlap with functionally annotated gene sets (CGP collection, N = 3302 gene sets) representing virtually all known biomolecular functions (Figure 2C). Strikingly, QT-A overlapped significantly with gene sets representing Polycomb targets and/or with trimethylated H3K27 (H3K27me3) mark in human embryonic stem (ES) cells that are related to cell proliferation and tumor development (eg, PRC2/SUZ12 targets, genes with H3K27me3, etc.), while QT-B was dominated by gene sets related to inflammatory response, NF-kappaB activity, EGF signaling and hypoxia (Figure 2C; Table S3). Notably, the

top-scoring gene in terms of correlation with the QT-B (ρ = 0.95; P = .001) was *PIK3C2A* which codes for a protein of the phosphoinositide 3-kinase (PI3K) family (Table S3). PI3K pathway is frequently altered in ovarian cancer and also in other cancer types, and is a driver of tumor formation and dissemination.[21] Noteworthy, QT-C overlapped with gene sets specifically expressed in stem cells (stromal and mammary), mesenchymal-like and nonproliferating cells, which are all hallmark of stemness (Figure 2C; Table S4), thus fulfilling our QT-C definition. Finally, we ran again the MSigDB analysis by using the H (hallmark) collection (N = 50 gene sets) which

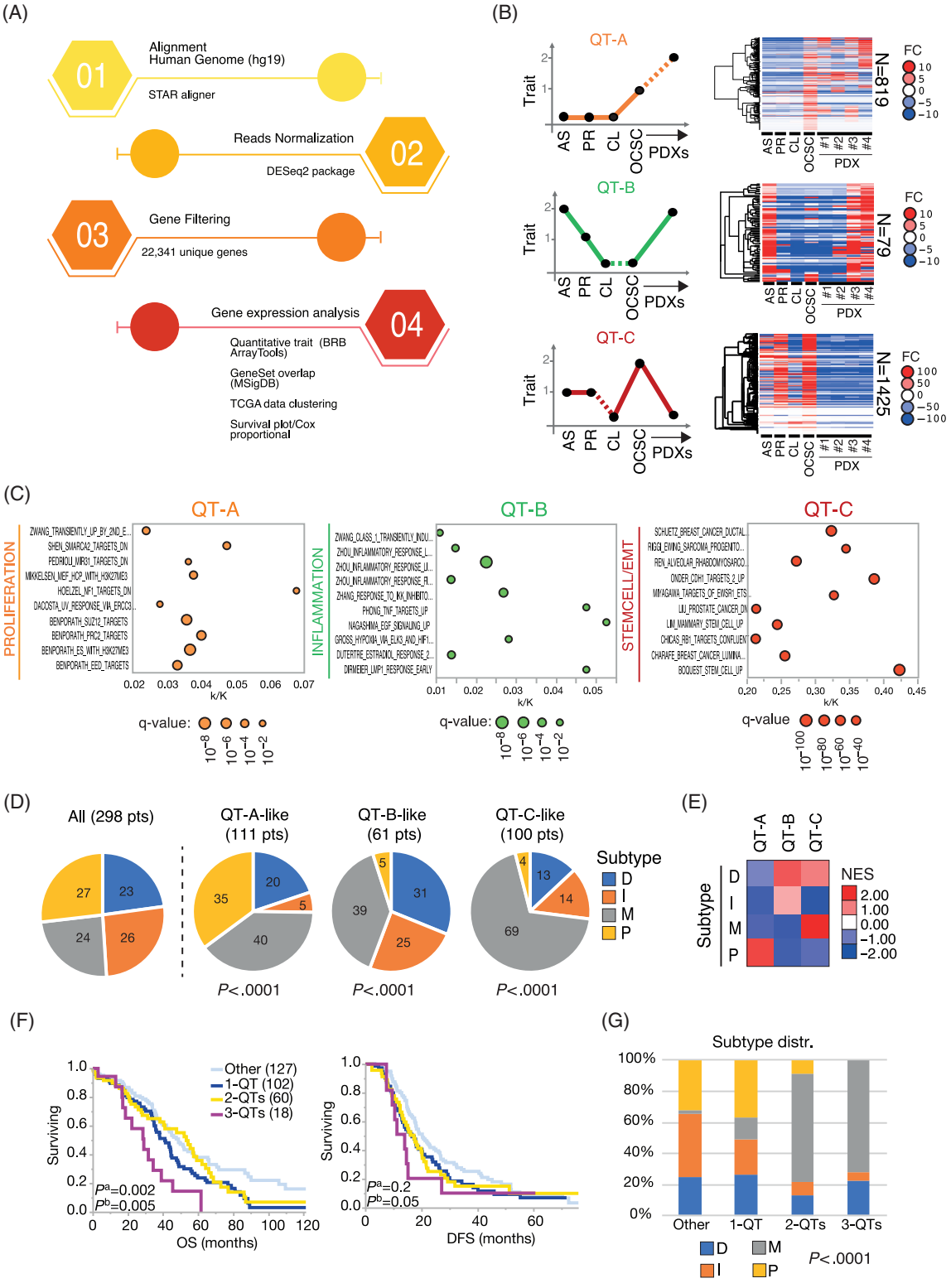

FIGURE 2 Legend on next page.

"summarizes and represents specific well-defined biological states."[22] Such analysis confirmed an enrichment for inflammatory and EMT-related gene sets in QT-B and QT-C, respectively (Table S4). The enrichment for inflammation-related gene sets in QT-B prompted us to further investigate the tissue-infiltrating immune and stromal cell populations in the As11-set. CIBERSORT and MCP-counter analyses (Section 2) revealed a heterogeneous infiltrate of immune cells in AS and also in PDXs but not, as expected, in PR. The presence of immune cell subpopulations in PDXs (Figure S3B, S3C) is consistent with the notion that SCID mice, that were used for the xenotransplantation, retain certain immune cells lineages.[23] The MCP-counter analysis also revealed the overrepresentation of fibroblast-associated genes in PR and OCSCs samples, while endothelial genes were not represented (Figure S3D). Given that no fibroblast contamination was observed in As11 primary culture (Section 2), this finding most likely reflects the mesenchymal (ie, fibroblast-like) features of PR and OCSC, in line with the expression of CD44, CD73 and vimentin (Figure S3A) as well as with previous characterization of OCSC-enriched spheroids.[13]

3.3 | As11-gene modules suggest mechanisms underpinning the HGSOC molecular subtypes

Recent studies on HGSOC transcriptome established the existence of at least four molecular subtypes, the proliferative, mesenchymal, immunoreactive and differentiated subtype, which correlate with prognosis.[17] We therefore aimed to verify whether QT-A, QT-B and QT-C are associated with HGSOC molecular subtypes, which would contribute to unveiling the pathobiological mechanisms that dominate the subtypes themselves. Hierarchical clustering analysis of the TCGA-HGSOC dataset[6] (N = 307; see Table S5 for a description of the cohort) scored clusters of tumors with an increased expression of QT-A, QT-B and QT-C genes (Figure S4A). Interestingly, the distribution of the HGSOC molecular subtypes[17] within the QT-A-, QT-B- and QT-C-like clusters of tumors deviated significantly from the expected distribution ($P < .0001$; Likelihood ratio test). As shown in Figure 2D, while all HGSOC molecular subtypes were represented in QTs, the proliferative subtype (P) was more represented in the QT-A-like cluster (ie, 35% vs 4%-5% in QT-B- and QT-C-like clusters), in line with the overrepresentation in QT-A of genes involved in cell proliferation and development (Figure 2C). Conversely, the percentages of tumors belonging to the immunoreactive (I) and differentiated subtypes (D) increased in the QT-B-like cluster (25% and 31%, respectively; Figure 2D). Strikingly, the majority of tumors in the QT-C-like cluster belonged to the mesenchymal subtype (M; 69%; Figure 2D). QT-C is enriched in genes associated with stem cells/EMT (Table S4) and is overrepresented in OCSCs (Figure 2B). This strongly suggests that the mesenchymal subtype of HGSOC is enriched in tumors with stem-like phenotype. To further validate our findings, we performed Gene-Set Enrichment Analysis (GSEA) using QT-A, QT-B and QT-C as gene sets. This confirmed the enrichment of QT-A genes in tumors of the proliferative subtype, QT-B genes in the differentiated tumors and QT-C genes in the mesenchymal tumors (Figures 2E and S4B).

We then asked whether the increased expression of QT-A, QT-B and QT-C genes in HGSOC was associated with patients' prognosis. HGSOC patients with concomitant increase in QT-A, QT-B and QT-C genes (ie, 3-QTs class) had the lowest survival as shown by Kaplan-Meier analysis ($P < .01$; Figure 2F) as well as by Cox proportional hazard model (HR = 3.29 [1.76-6.13]; Tables 1 and S6A). Contrariwise, HGSOC patients overexpressing neither QT-A, QT-B nor QT-C genes (ie, "Other" class) showed the most favorable prognosis (Figure 2F). Interestingly, patients belonging to 1-QT class, that is, with increased expression of only one QT (either A or B or C), showed an intermediate prognosis (Figure 2F; Tables 1 and S6A), while this was not always the case for patients with a combination of two QTs (ie, 2-QTs class; Figure 2F), probably due to unknown confounders. Notwithstanding, Cox analysis revealed that the average increase of HR was 23% ($P = .0120$) for each additional QT (Tables 1 and S6A).

Disease-free survival analysis revealed that no clinical and pathological parameters were a significant prognostic factor though we observed that the adjusted average risk-increase was borderline significant for an increasing number of QTs ($P = .07$; Figure 2F; Tables 2 and S6B). Finally, we interrogated the TCGA dataset to test whether the expression of the QTs could also give predictive information on the tumor response

FIGURE 2 Transcriptomic profiles of the As11-set. (A) Bioinformatic workflow for RNA-seq analysis. (B) Quantitative trait analysis (QT) of the ovarian cancer transcriptome over analyzed samples: tumor ascites (AS), primary cells (PR), established cell line (CL), stem cells (OCSCs) and patient-derived tumor xenografts (PDXs). QT-A, genes putatively involved in HGSOC initiation; QT-B, genes putatively involved in tumor-host interaction; QT-C, genes putatively involved in OCSC pathophysiology. Filled areas show the trend of global geometric means (geoM) of normalized reads (Reads; Y-axis) of expressed genes (ie, with >0 reads) in every QTs, to allow better quantitative assessment of regulation of QTs across samples. N, number of genes in each cluster. FC, fold change (median centered). (C) The Molecular Signature Database (MSigDB) analysis was performed as described in Methods using the gene sets C2-CGP database. The top 10 overlapping gene sets are displayed in a bubble plot where the size of bubbles indicates the significance (*q*-value) of overlapping as indicated in the legend. In the *X*-axis, the relative fraction of overlapping genes between the QT relative gene set (k) and C2-CGP gene set (K) is indicated. (D) Distribution of the HGSOC molecular subtypes in the TCGA HGSOC dataset (N = 298; left pie chart) and in the tumor subsets identified by QT-A, QT-B and QT-C. D, differentiated subtype (right charts); I, immunoreactive subtype; M, mesenchymal subtype; P, proliferating subtype. E) GSEA of QT-A, QT-B and QT-C in the various HGSOC tumor subtypes (see also Figure S4B). Heatmap illustrates the normalized enrichment score (NES) calculated by GSEA. NES values are as per the legend. (F) Survival analysis of TCGA HGSOC patients (N = 307) stratified by using QT-A, QT-B and QT-C (see Figure S4A and methods). 1-QT, patients with tumors overexpressing genes from only one QT among QT-A or QT-B, or QT-C. 2-QTs, patients with tumors overexpressing genes from two QTs (QT-A and QT-B, QT-B and QT-C, or QT-A and QT-C). 3-QTs, patients with tumors overexpressing genes from all three QTs. Other, patients with tumors not overexpressing QT-A-B-C genes. Left and right panels show overall survival (OS) and disease-free survival (DFS), respectively. Log-rank *P* values are displayed (P^a) together with linear trend *P* values (P^b)

TABLE 1 Univariate and multivariable Cox regression analysis for overall survival

	Univariate[a]		Multivariable[b]	
Overall survival	**HR (95% CI)**	**Wald test *P*-value**	**HR (95% CI)**	**Wald test *P*-value**
Age at surgery (1-year increase)	1.03 (1.01-1.04)	.0004	1.02 (1.01–1.04)	.0013
Grade G3 (vs G1-G2)	1.52 (0.97-2.41)	.07	1.73 (1.07-2.80)	.0267
Stage III-IV (vs I-II)	1.88 (0.88-4.00)	.10	1.63 (0.74-3.60)	.23
1-QT (vs other)	1.56 (1.11-2.20)	.0109	1.54 (1.08-2.19)	.0179
2-QTs (vs other)	1.32 (0.88-1.96)	.18	1.20 (0.80-1.80)	.37
3-QTs (vs other)	2.77 (1.52-5.06)	.0009	3.29 (1.76-6.13)	.0002
QT-1 unit increase	1.25 (1.07-1.47)	.0052	1.23 (1.05-1.45)	.0120

Note: Hazard ratio (HR) and 95% confidence interval (95% CI) were reported.
[a]Global test for QT class: $P = .0033$.
[b]Global test for QT class: $P = .0012$; nested likelihood ratio test after adding QT class: $P = .0009$.

TABLE 2 Univariate and multivariable Cox regression analysis for disease-free survival

	Univariate[a]		Multivariable[b]	
Disease-free survival	**HR (95% CI)**	**Wald test *P*-value**	**HR (95% CI)**	**Wald test *P*-value**
Age at surgery (1-year increase)	1.01 (0.99-1.02)	.31	1.01 (0.99-1.02)	.41
Grade G3 (vs G1-G2)	1.25 (0.81-1.92)	.31	1.19 (0.73-1.92)	.48
Stage III-IV (vs I-II)	1.60 (0.91-2.81)	.10	1.56 (0.83-2.93)	.17
1-QT (vs other)	1.33 (0.94-1.89)	.10	1.39 (0.97-2.00)	.08
2-QTs (vs other)	1.30 (0.88-1.91)	.19	1.22 (0.82-1.81)	.32
3-QTs (vs other)	1.73 (0.86-3.45)	.12	1.98 (0.97-4.04)	.06
QT-1 unit increase	1.17 (1.00-1.37)	.05	1.16 (0.99-1.37)	.07

Note: Hazard ratio (HR) and 95% confidence interval (95% CI) were reported.
[a]Global test for QT class: $P = .21$.
[b]Global test for QT class: $P = .14$; nested likelihood ratio test after adding QT class: $P = .07$.

to platinum-based chemotherapy. Indeed, the majority of platinum-resistant patients had an increased expression of at least one QT (32 out of 43, ~74%; Table S5) while most of the patients not over-expressing any QTs (54 out of 65, ~83%; Table S5) were among the chemosensitive group. Such results were confirmed also by univariate and multivariate logistic analysis, with chemoresistance increasing by approximately 1.6 Odds for each QT unit increase (Table S6C).

3.4 | The mutational landscape of As11-set reveals cancer driver mechanisms involved in HGSOC stemness and progression

We then investigated the mutational profiles of As11-set. The bio-informatics workflow of this analysis is outlined in Figure 3A. The whole-exome DNA-seq analysis yielded an average of ~32 million reads, with an average of 1.8 SNVs/Mb and ~70 de novo mutations, which is in line with the TCGA-HGSOC exome sequencing analysis.[6] We also verified the fraction of reads from xenograft sources in PDXs by using the Xenome software[24] (Section 2). Less than 1% (0.41%-0.93%) of PDX-derived reads belonged either to mouse or both human and mouse, which we therefore considered as negligible in our analyses. Next, by using patient-matched blood samples as normal, nontumor counterpart, we identified 2053 somatic variants that were exonic, nonsynonymous and present in at least two samples among AS-derived aggregates, PR and OCSCs (Figure 3A; Table S7A). Our mutation analysis also entailed variants present in the dbSNP database given that somatic cancer-related mutations have been found in this database.[25] Overall, the pattern of mutational substitutions was enriched for C>T (Figure 3B), consistently with other HGSOC-associated mutational profiles reported previously,[5] while other mutational substitutions occurred at a lower percentage (Figure 3B).

A high number of mutations (N = 693; 522 genes) were shared by all samples (in green in Figure 3C), including a nonsense mutation in the *TP53* gene classified as pathogenic (COSMIC; FATHMM score = 1.00; Table S7B). However, we also found two groups of mutations which diverged: (i) 30 mutations were common to OCSCs, PR and PDXs (in pink in Figure 3C); (ii) 355 mutations were shared between OCSCs and PR only (in yellow in Figure 3C). Notably, among

the mutations shared by all samples of As11-set, the variant allele frequency (indicated by green bars in Figure 3C) increased markedly in PR, OCSCs and PDXs as compared to the original ascites. Gene Ontology (GO) analysis of the 522 shared mutated genes showed that the five most enriched pathways were all involved in cell adhesion (Table S8), a process that is highly relevant in cancer progression.[26]

It is worth noting that genetic heterogeneity in ascites gradually decreased in PR, OCSCs and PDXs samples (Figure S5), which suggests that a subset of tumor cells with peculiar genetic characteristics expanded in OCSCs and in PDXs. Since ascites are fluid and neither the primary tumor nor matched metastases were available, it was not possible to perform a typical clonal evolution analysis, which could help to identify cancer driver mutations.[27,28] Therefore, we hypothesized that

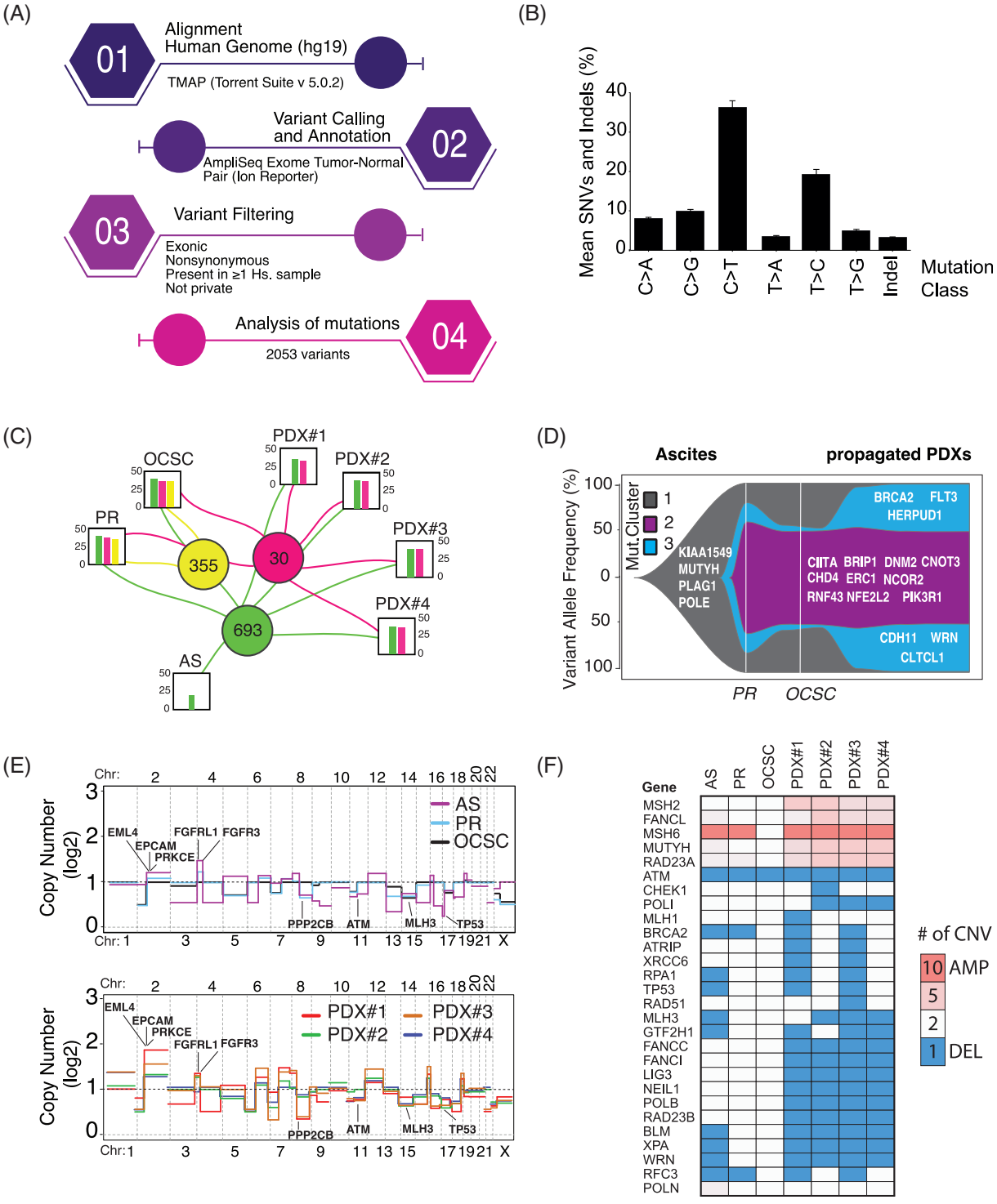

FIGURE 3 Legend on next page.

the cancer driver mutations relevant for HGSOC progression and OCSC function might be those emerging in OCSCs and in serially transplanted PDXs. Using this strategy, we identified three main clusters of mutations in ascites that exhibited different frequency profiles in the other As11-derived samples (Figure 3D): (i) the "MutCluster 1", containing mutations detectable in the bulk of ascites cells and in all other samples (N = 159, Table S7A); (ii) the "MutCluster 2", containing less frequent mutations in the bulk of ascites cells which then expanded in PR and OCSCs and were retained in PDX samples (N = 903, Table S7A); (iii) the "MutCuster 3", containing less frequent mutations in the ascites which then expanded in PR and OCSCs and further enriched in PDX samples (N = 220, Table S7A). By analyzing these MutClusters we identified several mutations in cancer-associated genes, such as (i) *POLE*, encoding the DNA polymerase ε, which is involved in DNA repair and is frequently mutated in different OC histotypes[29] (MutCluster1); (ii) *PIK3R1*, which encodes the 85 kDa (p85) regulatory subunit of Phosphatidylinositol 3-kinase (PI3K) (MutCluster2); (iii) *BRCA2*, that is involved in homologous recombination pathway for double-strand DNA repair and is frequently altered in HGSOC (MutCluster3). Other mutations in tumor suppressor genes or oncogenes present within the Cancer Gene Census of the COSMIC database[30] were also identified, such as *CDH4*, *RNF43*, *RGPD3*, *CDH11*, *DNM2* and *FLT3* (Figure 3D). Interestingly, we also found mutations in the *PIK3R1* gene (coding for the PI3K p85 regulatory subunit) that were located in hotspots of Src homology 2 (SH2) regions, that is, the N-term (nSH2) and inter-SH2 (iSH2; Figure S6A).

Finally, we profiled the copy number variations (CNV) of the bulk ascites cells, primary cells and OCSCs, and found that several CNV involved oncogenes and tumor suppressor genes (Figure 3E; Table S9). Among them, *TP53* and *ATM* were in deleted regions while the chromosomal regions containing *FGFRL1*, *FGFR3* and *EPCAM* were amplified (Figure 3E). Of note, *TP53* and *ATM* are involved in DNA damage responses like *BRCA2* and *POLE*, which we found mutated. Alterations in DNA damage repair and response genes are a hallmark of ovarian cancer.[6,31] As a matter of fact, we observed frequent deletion of genes implicated in homologous recombination (ie, *BRCA2* and *FANCI*), base and nucleotide excision repair (ie, *XPA* and *NEIL3*), nonhomologous end-joining (*WRN*), and DNA damage signaling (ie, *TP53*, *ATM* and *FANCC*; Figure 3F).

Our strategy, therefore, revealed CNVs and mutations in several cancer driver genes relevant for HGSOC progression. Of note, we found less frequent mutations in AS that expanded in PR and OCSCs and were retained in PDXs (ie, MutCluster 2).

Importantly, we scored mutations in nSH2 and iSH2 domains of PIK3R1 associated to loss of function of the PI3K p85 regulatory subunit which unleashes the p110 (PI3K) catalytic activity,[32] particularly in tumors with PTEN heterozygous mutations.[33] Genetic alterations in PI3K signaling pathway were indeed described in the TCGA HGSOC cohort of patients (Figure S6B). We thus explored whether PI3K signaling and function were altered in As11-derived PR and OCSCs.

3.5 | PIK3R1 mutation is accompanied by PI3K addiction in OCSCs

The enrichment for *PIK3R1* mutation in OCSCs might result in deregulated PI3K signaling in OCSCs. To test this hypothesis, we investigated the contribution of PI3K activity to spheroid formation by primary As11 cells, using the PI3K inhibitor LY294002. First, we verified that LY294002 prevented serum-induced AKT phosphorylation, a key step in the PI3K cascade, in PR (Figure 4A), which confirmed the ability of the compound to inhibit PI3K signaling. Strikingly, LY294002 abrogated completed the spheroid-forming capability of PR (Figure 4B). This finding was also validated with two additional PI3K inhibitors, alpelisib and copanlisib, which also reduced spheroid formation in PR in a dose-dependent manner (Figure S7). Furthermore, LY294002 induced the downregulation of a panel of EMT/stem-cell markers (Figure S2C) in formed spheroids, thus implicating PI3K signaling in both spheroid generation and stem trait maintenance. Notably, LY294002 treatment of adherent cells did not exert similar effects on EMT/stem-cell markers expression regulation (Figure S2D). The same assay was also performed on two primary cell cultures derived from different HGSOC samples (As91 and As40) which exhibited no mutations in *PIK3R1* or in other genes associated with PI3K signaling (data not shown). In this case, the efficiency of LY294002 in preventing spheroid formation was remarkably lower than in PR (Figure 4C). This suggests that a PIK3R1-inactivating mutation renders OCSCs dependent on PI3K activity at least for some stemness-related properties. Interestingly, LY294002 inhibited the proliferation of primary HGSOC cells in 2D cultures with comparable efficiency in PR and in PIK3R1-wild-type cells (Figure 4D).

FIGURE 3 Genomic profiles of the As11-set. (A) Bioinformatic workflow for DNA-seq analysis. (B) Pattern of mutational substitutions identified in the As11 samples by DNA-seq whole-exome profile analysis. Bar plot indicates the average percentage of SNV and Indel over the samples analyzed (N = 7). Error bars indicate relative standard errors. (C) Distribution of the somatic mutations across all sample types. Colored circles in the middle represent the total number of mutations identified in all samples (green), or private to primary cells (PR), OCSCs and PDXs (pink) or private to primary cells and OCSCs (yellow). AS, tumor ascites. Colored histograms represent the average of the variant allele frequency in percentage. (D) Estimation of the molecular heterogeneity using clonevol R package and fish plot. PyClone analysis revealed three potential clusters (Mut. Cluster 1-2-3, gray, purple and blue, respectively) which are enriched in mutations with a diverse allele frequency in the different sample types. The indicated genes belong to the Cancer Gene Census of COSMIC database. *Y*-axis, variant allele frequency (%). (E) Somatic copy number variants (CNV) were identified in the sequenced samples. *Top panel*: CNV in tumor ascites (AS), primary cells (PR) and stem cells (OCSCs); *Bottom panel*: CNV in the serial PDX samples. *Y*-axis, number of copies (Log2). *X*-axis, chromosomal position. Black dashed line indicates the diploid status. Gene symbols represent oncogenes or tumor suppressor genes (Section 2) with an altered copy number profile shared in at least two samples. (F) Heatmap representing CNA of genes involved in DNA repair mechanisms across As11 sample types. Copy number values are as per the legend

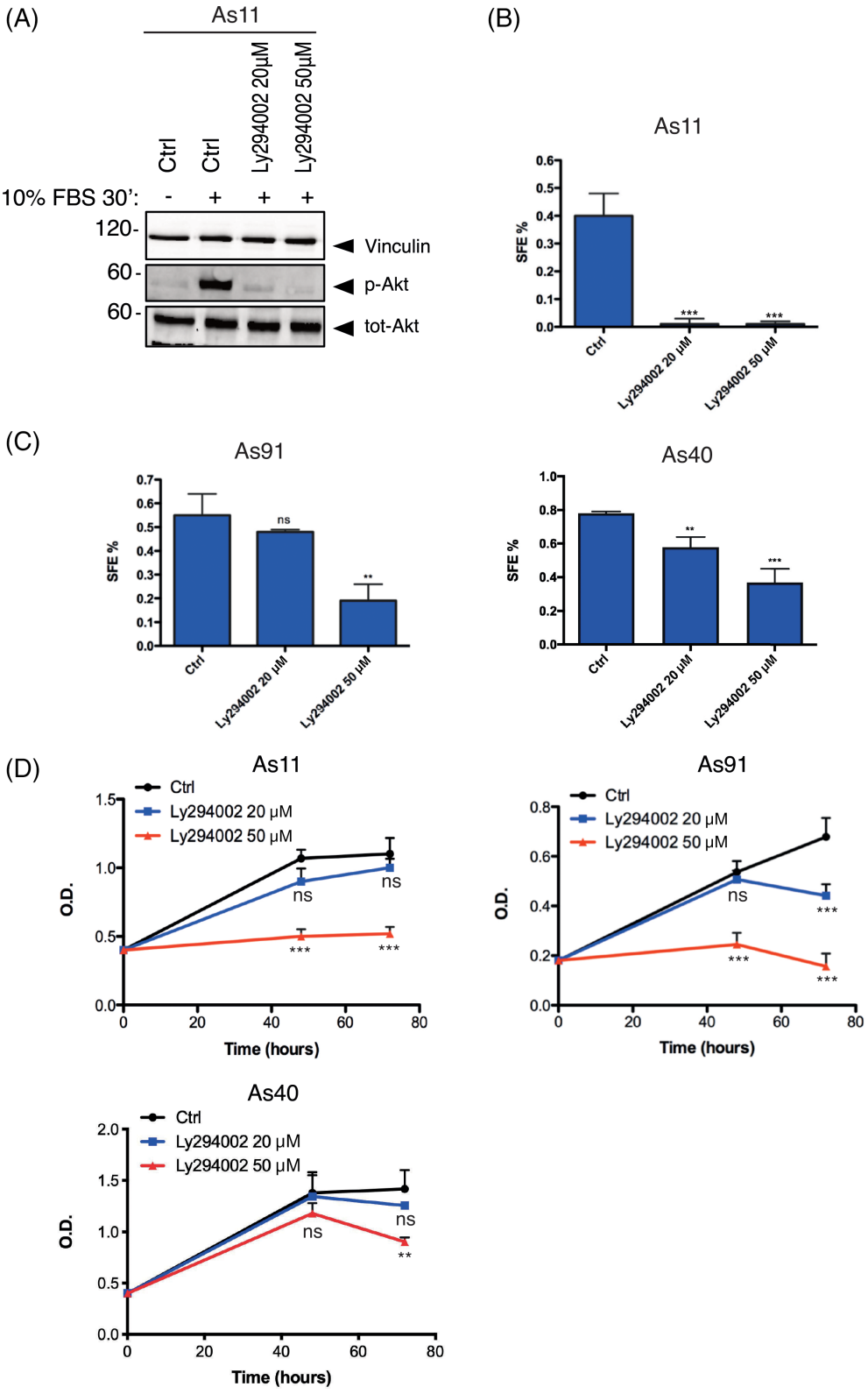

FIGURE 4 Role of the *PIK3R1* mutation in OCSCs. (A) Early-passage primary As11 cells were stimulated for 30 minutes with 10% fetal bovine serum either in the absence or in the presence of 20 or 50 μM LY294002. Cell extracts were immunoblotted for phospho-AKT (p-AKT), total AKT, using vinculin as equal loading control. (B) Primary As11 cells were cultured under nonadherent and serum-free conditions and allowed to form OCSC-enriched spheroids either in the absence or in the presence of LY294002 at 20 or 50 μM. (C) The same conditions were applied to As91 and As40, two additional primary HGSOC cell cultures that did not have *PIK3R1* mutations. (D) Cell proliferation assay on early-passage primary As11, As91 and As40 cells either in the absence or in the presence of LY294002 at 20 or 50 μM. (ns, not significant; $^{**}P < .001$; $^{***}P < .0001$) [Color figure can be viewed at wileyonlinelibrary.com]

4 | DISCUSSION

High-grade serous ovarian carcinoma is an aggressive disease that rapidly progresses to metastatic cancer and disseminates into the abdominal cavity. Treatment of ovarian cancer is challenging due to frequent relapse and acquirement of chemotherapy resistance. Our scant knowledge of the molecular features of ovarian cancer metastases and OCSCs, which are at the basis for tumor development, metastasis and chemotherapy resistance, is actually limiting the development of effective therapeutic strategies for HGSOC patients.

We thus reasoned that a direct and in-depth investigation of the transcriptional and mutational landscape of cancer cells and OCSCs isolated from malignant ascites could definitely help to identify molecular mechanisms relevant for HGSOC biology and oncology. We have performed also a PDX serial transplantation assay using ascites-derived tumor spheroids to model the tumor metastatic re-seeding capacity with the aim to capture relevant mechanisms in HGSOC dissemination. Gene expression analysis of this sample series revealed the existence of at least three clusters of genes (QT-A, QT-B and QT-C) that we found enriched in genes associated with cancer development, tumor-host response and stemness, respectively. Unexpectedly, when we looked at the expression profile of QT-A, QT-B and QT-C in the large cohort of HGSOC samples profiled by TCGA (N = 307), we observed sizable clusters of tumors which over-expressed a significant fraction of QT-A, QT-B and QT-C genes (Figure S4A). This finding suggests that despite the As11-set of tumor samples was derived from a single HGSOC patient, our experimental system was powerful enough to capture molecular features representative of the disease. Our approach, being based on a well-controlled experimental setting, enables to predict the predominant biomolecular traits of these tumor clusters identified in the TCGA dataset. For example, (i) tumors of the QT-A-like cluster (Figure S4A) are expected to have an altered control of lineage and differentiation determinants because most of QT-A genes are related to the Polycomb-group signaling (SUZ12, EED and PRC2; Figure 2C), which in cancer could lock cells in an undifferentiated/proliferative state. It is noteworthy, in this context, that QT-A genes are upregulated in OCSCs and in serially propagated PDX (Figure 2B). (ii) Tumors of the QT-B-like cluster appeared to have an inflammatory phenotype as anticipated by the upregulation in QT-B of genes involved in the inflammatory response (Figure 2C; Table S4). Accordingly, we found QT-B genes upregulated in cancer cells freshly isolated from ascites, consistent with the latter being a highly inflammatory environment,[19,20] and then downregulated in vitro in monoculture condition were stromal/inflammatory cells are lacking, as shown also by our CIBERSORT and MCP-counter analyses (Figure S3B,C). Finally, (iii) tumors of the QT-C-like cluster appeared to be dominated by a cancer stem-cell phenotype due to the upregulation of several genes involved in stem cell biology (Figure 2C) and EMT (eg, Zeb1, Zeb2, Slug, Twist1, Twist2; Tables S2 and S3), which indeed we found specifically overexpressed in OCSCs.

These findings were further supported when our analysis was extended to the Consensus Ovarian Cancer Subtypes.[34] Indeed, the proliferative subtype was predominant in QT-A-like cluster, the inflammatory subtype was enriched in QT-B-like cluster, and the mesenchymal subtype was more prevalent in the QT-C-like group, which is indeed characterized by stem-cell/EMT related genes. Of note, we propose here for the first time that the mesenchymal subtype, that was originally associated with tumors with an increased stromal component, is specifically enriched in tumors with stem-like phenotype, as indicated by the upregulation of genes that we found associated with OCSCs. Notably, in HGSOC multiple subtype-specific gene signatures can be expressed simultaneously in a tumor, suggesting that different molecular subtypes coexist in a HGSOC, most likely contributing to determine its phenotype and aggressiveness.[17] In line with this assumption, we observed a clear association of the simultaneous presence of QT-A, QT-B and QT-C signatures with a poor prognosis in HGSOC patients. Overall, these data unveiled a certain plasticity in malignant ascites which can trigger several pathways ultimately contributing to enhance HGSOC aggressiveness.

In the last years, several studies provided insights on the ovarian cancer genetics, frequently characterized by ubiquitous *TP53* mutations and by the inactivation of the homologous recombination repair mechanisms, best exemplified by *BRCA1/2* alterations.[5,6] Apart from *TP53* mutations, point mutations in cancer driver genes are rare in primary HGSOC: approximately one-third of primary HGSOC have no detectable genetic alterations in cancer genes known to be relevant in metastatic progression and chemoresistance.[6,35,36] While cancer driver genes in HGSOC are more frequently altered by structural rearrangements,[36] we believe that the high intratumor heterogeneity typical of primary HGSOC[6] would complicate the identification of the cancer driver lesions carried by the "born-to-be-bad" tumor cell subpopulation, that is, those cancer cells with an ab initio metastatic advantage. Our strategy integrated the analysis of the metastatic cancer cells in ascites, which by definition represent the evolved "born-to-be-bad" subpopulation, with that of cancer cells capable of self-renewing (ie, the OCSCs) and/or of re-initiating a HGSOC (ie, the orthotopic PDX model). We propose that such a workflow provides molecular insights into the ovarian cancer progression and allows to identify relevant cancer driver mutations. Indeed, we found several mutations which were subclonal in malignant ascites and then emerged in OCSCs and in serially transplanted PDXs, affecting known cancer genes (*BRCA2*, *POLE*, *FLT3*, *NFE2L2*, *BRIP1*, *PIK3R1*, etc.), which suggests a role for these mutations as drivers in cancer stem cells and HGSOC progression.

Although we acknowledge that NGS analysis of different sample types from a single tumor can provide limited information on the mutational landscape of metastatic HGSOC, we were confident about the relevance of our results based on previous studies. For example, Ding et al applied a similar approach, sequencing multiple sample types from one breast cancer patient, and identified driver mutations that could be validated in larger cohorts of patients.[37] Notably, the high genetic heterogeneity found at the primary site decreased markedly in brain metastasis and xenograft samples,[37] arguing that a subset of tumor cells expanded during metastatic spread in the patient and tumor propagation in mice. This is in agreement with our data, which revealed a reduction in genetic heterogeneity inferred from the distribution of frequencies among ascites, PR, OCSCs and PDXs (Figure S5). In this context, it is also noteworthy that the somatic mutation prevalence (1.8 SNVs/Mb) and the predominant pattern of mutational substitutions (C>T) emerged in our study were in line with the TCGA exome sequencing analysis of a large set of HGSOCs. Furthermore, the CNV analysis of As11-set confirmed the frequent deletion of genes implicated in DNA repair mechanisms that is indeed a hallmark of HGSOC.[5,6,36] Finally, our approach was further supported by other studies that also relied on the analyses of intrapatient matched tumor

samples from a single cancer patient[38] or in very small cohorts of patients and, nevertheless, provided insights into fundamental cancer biology with relevant therapeutic implications.[27,39,40]

Among the cancer driver mutations identified, we focused on those on the *PIK3R1* gene. Overall, *PIK3R1* is altered in a small subset of human tumors (~3%; MSK-IMPACT Clinical Sequencing Cohort, N = 10 945 samples[41]). An alteration frequency of 2.8% is found in HGSOC (Figure S6B), while it is higher in other ovarian cancer subtypes such as clear cell carcinoma.[33,42] *PIK3R1* codes for the p85α regulatory subunit of the PI3K enzyme which modulates the activity of the p110α catalytic subunit. In particular, p85α is considered a tumor suppressor since it stably binds to p110α through the SH2 domains and inhibits its activation.[43] In our experimental setting, we identified mutations in the iSH2 domain (nonframeshift insertion, N453_T454insL) and in the nSH2 domain (frameshift deletion, I381fs). In agreement with our findings, a pan-cancer analysis revealed that *PIK3R1* is deleted or mutated in hot spots regions located in the iSH2 and, to a lesser extent, in the nSH2 domain (MSK-IMPACT Clinical Sequencing Cohort and COSMIC; Figure S6B). Mutations in the SH2 domains disrupt the interaction of p85α with p110α, relieving the repressive action on the catalytic subunit and ultimately leading to PI3K hyperactivation.[43]

In fact, the role of PI3K signaling as a tumor promoter in ovarian cancer has long been established. Aberrant PI3K activation sustains tumor cell survival and drug resistance and, hence, blockade of the pathway has been widely explored as a therapeutic strategy in preclinical systems.[21] Further evidence on this has been recently obtained through the identification of a novel *PIK3R1* mutation in a HGSOC case. Unlike As11, the mutation affected the cSH2 domain of p85α, nevertheless, the functional outcome was again an excessive PI3K activation, which proved to be a druggable alteration.[44] Our study extended the previous observations on the link between PI3K and ovarian malignancy by unveiling the role of mutant *PIK3R1* and aberrant PI3K signaling in OCSCs function. While earlier reports have implicated the PI3K pathway in the expression of stem-associated markers in ovarian cancer cells[45] as well as in ovarian tumor initiation,[46] we provide the first demonstration that it is actually required for stemness-related functional properties such as resistance to *anoikis* and self-renewal (as reflected by spheroid formation ability). We also made the intriguing observation that *PIK3R1*-mutant HGSOC cells become addicted to PI3K signaling for spheroid formation, while this is not the case for *PIK3R1*-wild-type cells. Conversely, PI3K signaling is required for cell proliferation independent of the *PIK3R1* status. The biological mechanisms that underlie the specific impact of mutant *PIK3R1* (and, by enlarge, of an aberrant PI3K pathway) on HGSOC stem-like properties remain elusive and warrant further investigation. Regardless, these findings imply that the therapeutic inhibition of PI3K signaling might offer the dual advantage of restraining tumor growth and preventing OCSCs-driven events such as metastasis initiation and tumor recurrence. Along the same line, OCSCs are viewed as main players in chemoresistance[12] and PI3K signaling confers drug resistance to ovarian cancer cells.[47,48] Thus, it is tempting to speculate that PI3K inhibition could overcome OCSCs-driven chemoresistance, an hypothesis that deserves further investigation given its potential implications for the clinical management of ovarian cancer patients.

Therefore, we have delineated a workflow that, through the integrated genomic and transcriptomic profiling of multiple sample types derived from a single HGSOC case, revealed molecular alteration patterns that proved prognostic and predictive value in HGSOC patients. As exemplified by the *PIK3R1* mutation and PI3K deregulation in OCSCs, our approach can identify actionable alterations that may offer new therapeutic options.

ACKNOWLEDGEMENTS

This paper is dedicated to the memory of the patient who donated her samples for this study. Fabrizio Bianchi wishes to dedicate this work to the memory of Lucia, an extraordinary girl who experienced cancer as an opportunity to entrust her and all her loved ones to the love of the Father. We are grateful to R. M. Carletti, E. Marino and G. Jodice for technical assistance, V. Das and E. Villa for contribution to data analysis, S. Pece for support, N. Colombo and the Ovarian Cancer Center staff at IEO (Milano) for providing the As11 sample and associated clinical data. This work was supported by Associazione Italiana Ricerca sul Cancro (IG-14622 and IG-21320 to Ugo Cavallaro, MFAG-17568 and IG-22827 to Fabrizio Bianchi, IG-2017 to Giuseppe Testa, IG-23250 to Raffaella Giavazzi), the Italian Ministry of Health (RF-2016-02362551 to Ugo Cavallaro, GR-2016-02363975 and CLEARLY to Fabrizio Bianchi), Fondazione Istituto Europeo di Oncologia-Centro Cardiologico Monzino (grant to Ugo Cavallaro), Roche per la Ricerca (grant to Michela Lupia). Michela Lupia was supported by fellowships from Fondazione Istituto Europeo di Oncologia-Centro Cardiologico Monzino and Fondazione Umberto Veronesi. Pietro Lo Riso was supported by fellowships from Fondazione Istituto Europeo di Oncologia-Centro Cardiologico Monzino and Fondazione Italiana per la Ricerca sul Cancro.

CONFLICT OF INTEREST

The authors declare that they have no conflict of interest.

AUTHOR CONTRIBUTIONS

Conception and design: Ugo Cavallaro, Fabrizio Bianchi; *Development of methodology*: Michela Lupia, Valentina Melocchi, Fabrizio Bianchi, Ugo Cavallaro; *Acquisition of data*: Michela Lupia, Valentina Melocchi, Francesca Bizzaro, Pietro Lo Riso, Alberto Ranghiero, Micol Baronio, Fabrizio Bianchi; *Analysis and interpretation of data*: Michela Lupia, Valentina Melocchi, Francesca Bizzaro, Pietro Lo Riso, Elisa Dama, Micol Baronio, Alberto Ranghiero, Massimo Barberis, Loris Bernard, Giovanni Bertalot, Raffaella Giavazzi, Giuseppe Testa, Fabrizio Bianchi, Ugo Cavallaro; *Writing, review and/or revision of the manuscript*: Michela Lupia, Valentina Melocchi, Fabrizio Bianchi, Ugo Cavallaro; *Administrative, technical or material support*: Loris Bernard, Massimo Barberis; *Study supervision*: Ugo Cavallaro, Fabrizio Bianchi. The work reported in the paper has been performed by the authors, unless clearly specified in the text.

DATA AVAILABILITY STATEMENT

Raw and normalized RNA-seq data generated in our study are available in the Gene Expression Omnibus (GEO; https://www.ncbi.nlm.nih.gov/geo) with accession number: GSE154950. The raw DNA-seq data are available in Sequence Read Archive (SRA; https://www.ncbi.nlm.nih.gov/sra) with accession number: PRJNA655814. Other data that support the findings of our study are available from the corresponding authors upon request.

ETHICS STATEMENT

Informed consent was obtained from the patients in the study. Our study was performed in accordance with the Declaration of Helsinki and was approved by the European Institute of Oncology Ethics Committee (protocol no. R789-IEO). Animal studies were performed following a protocol approved by the fully authorized animal facility of Istituto di Ricerche Farmacologiche Mario Negri and by the Italian Ministry of Health (as required by the Italian Law) (protocol no. 945/2016-PR) and in accordance with EU directive 2010/63.

ORCID

Massimo Barberis https://orcid.org/0000-0002-0943-4804
Raffaella Giavazzi https://orcid.org/0000-0001-5249-8208
Giuseppe Testa https://orcid.org/0000-0002-9104-0918
Ugo Cavallaro https://orcid.org/0000-0002-0884-6460

REFERENCES

1. Bray F, Ferlay J, Soerjomataram I, Siegel RL, Torre LA, Jemal A. Global cancer statistics 2018: GLOBOCAN estimates of incidence and mortality worldwide for 36 cancers in 185 countries. *CA Cancer J Clin*. 2018;68:394-424.
2. Pavlik EJ, Smith C, Dennis TS, et al. Disease-specific survival of type I and type II epithelial ovarian cancers-stage challenges categorical assignments of indolence & aggressiveness. *Diagnostics (Basel)*. 2020;10:56.
3. Torre LA, Trabert B, DeSantis CE, et al. Ovarian cancer statistics, 2018. *CA Cancer J Clin*. 2018;68:284-296.
4. McPherson A, Roth A, Laks E, et al. Divergent modes of clonal spread and intraperitoneal mixing in high-grade serous ovarian cancer. *Nat Genet*. 2016;48:758-767.
5. Eckert MA, Pan S, Hernandez KM, et al. Genomics of ovarian cancer progression reveals diverse metastatic trajectories including intraepithelial metastasis to the fallopian tube. *Cancer Discov*. 2016;6:1342-1351.
6. Cancer Genome Atlas Research Network. Integrated genomic analyses of ovarian carcinoma. *Nature*. 2011;474:609-615.
7. Tan TZ, Miow QH, Huang RY, et al. Functional genomics identifies five distinct molecular subtypes with clinical relevance and pathways for growth control in epithelial ovarian cancer. *EMBO Mol Med*. 2013;5:1051-1066.
8. Bregenzer ME, Horst EN, Mehta P, Novak CM, Repetto T, Mehta G. The role of cancer stem cells and mechanical forces in ovarian cancer metastasis. *Cancers (Basel)*. 2019;11:1008.
9. Ford CE, Werner B, Hacker NF, Warton K. The untapped potential of ascites in ovarian cancer research and treatment. *Br J Cancer*. 2020;123:9-16.
10. Kim S, Kim S, Kim J, et al. Evaluating tumor evolution via genomic profiling of individual tumor spheroids in a malignant ascites. *Sci Rep*. 2018;8:12724.
11. Carden CP, Stewart A, Thavasu P, et al. The association of PI3 kinase signaling and Chemoresistance in advanced ovarian cancer. *Mol Cancer Ther*. 2012;11:1609-1617.
12. Lupia M, Cavallaro U. Ovarian cancer stem cells: still an elusive entity? *Mol Cancer*. 2017;16:64.
13. Lupia M, Angiolini F, Bertalot G, et al. CD73 regulates stemness and epithelial-mesenchymal transition in ovarian cancer-initiating cells. *Stem Cell Rep*. 2018;10:1412-1425.
14. Francavilla C, Lupia M, Tsafou K, et al. Phosphoproteomics of primary cells reveals druggable kinase signatures in ovarian cancer. *Cell Rep*. 2017;18:3242-3256.
15. Massazza G, Tomasoni A, Lucchini V, et al. Intraperitoneal and subcutaneous xenografts of human ovarian carcinoma in nude mice and their potential in experimental therapy. *Int J Cancer*. 1989;44:494-500.
16. Ricci F, Bizzaro F, Cesca M, et al. Patient-derived ovarian tumor xenografts recapitulate human clinicopathology and genetic alterations. *Cancer Res*. 2014;74:6980-6990.
17. Verhaak RGW, Tamayo P, Yang J-Y, et al. Prognostically relevant gene signatures of high-grade serous ovarian carcinoma. *J Clin Invest*. 2013;123:517-525.
18. Simon R, Lam A, Li M-C, Ngan M, Menenzes S, Zhao Y. Analysis of gene expression data using BRB-array tools. *Cancer Inform*. 2007;3:117693510700300.
19. Matte I, Lane D, Laplante C, Rancourt C, Piché A. Profiling of cytokines in human epithelial ovarian cancer ascites. *Am J Cancer Res*. 2012;2:566-580.
20. Kim S, Kim B, Song YS. Ascites modulates cancer cell behavior, contributing to tumor heterogeneity in ovarian cancer. *Cancer Sci*. 2016;107:1173-1178.
21. Huang T-T, Lampert EJ, Coots C, Lee J-M. Targeting the PI3K pathway and DNA damage response as a therapeutic strategy in ovarian cancer. *Cancer Treat Rev*. 2020;86:102021.
22. Liberzon A, Birger C, Thorvaldsdóttir H, Ghandi M, Mesirov JP, Tamayo P. The molecular signatures database hallmark gene set collection. *Cell Syst*. 2015;1:417-425.
23. Vladutiu AO. The severe combined immunodeficient (SCID) mouse as a model for the study of autoimmune diseases. *Clin Exp Immunol*. 1993;93:1-8.
24. Conway T, Wazny J, Bromage A, et al. Xenome—a tool for classifying reads from xenograft samples. *Bioinformatics*. 2012;28:i172-i178.
25. Jung H, Bleazard T, Lee J, Hong D. Systematic investigation of cancer-associated somatic point mutations in SNP databases. *Nat Biotechnol*. 2013;31:787-789.
26. Dongre A, Weinberg RA. New insights into the mechanisms of epithelial-mesenchymal transition and implications for cancer. *Nat Rev Mol Cell Biol*. 2019;20:69-84.
27. Gerlinger M, Rowan AJ, Horswell S, et al. Intratumor heterogeneity and branched evolution revealed by multiregion sequencing. *N Engl J Med*. 2012;366:883-892.
28. Yates LR, Gerstung M, Knappskog S, et al. Subclonal diversification of primary breast cancer revealed by multiregion sequencing. *Nat Med*. 2015;21:751-759.
29. Wang YK, Bashashati A, Anglesio MS, et al. Genomic consequences of aberrant DNA repair mechanisms stratify ovarian cancer histotypes. *Nat Genet*. 2017;49:856-865.
30. Sondka Z, Bamford S, Cole CG, Ward SA, Dunham I, Forbes SA. The COSMIC cancer gene census: describing genetic dysfunction across all human cancers. *Nat Rev Cancer*. 2018;18:696-705.
31. George J, Alsop K, Etemadmoghadam D, et al. Nonequivalent gene expression and copy number alterations in high-grade serous ovarian cancers with BRCA1 and BRCA2 mutations. *Clin Cancer Res*. 2013;19:3474-3484.
32. Vallejo-Díaz J, Chagoyen M, Olazabal-Morán M, González-García A, Carrera AC. The opposing roles of PIK3R1/p85α and PIK3R2/p85β in cancer. *Trends Cancer*. 2019;5:233-244.
33. Cheung LWT, Hennessy BT, Li J, et al. High frequency of PIK3R1 and PIK3R2 mutations in endometrial cancer elucidates a novel

mechanism for regulation of PTEN protein stability. *Cancer Discov*. 2011;1:170-185.
34. Chen GM, Kannan L, Geistlinger L, et al. Consensus on molecular subtypes of high-grade serous ovarian carcinoma. *Clin Cancer Res*. 2018; 24:5037-5047.
35. Ciriello G, Miller ML, Aksoy BA, Senbabaoglu Y, Schultz N, Sander C. Emerging landscape of oncogenic signatures across human cancers. *Nat Genet*. 2013;45:1127-1133.
36. The Australian Ovarian Cancer Study Group, Patch A-M, Christie EL, et al. Whole-genome characterization of chemoresistant ovarian cancer. *Nature*. 2015;521:489-494.
37. Ding L, Ellis MJ, Li S, et al. Genome remodelling in a basal-like breast cancer metastasis and xenograft. *Nature*. 2010;464:999-1005.
38. Jiménez-Sánchez A, Memon D, Pourpe S, et al. Heterogeneous tumor-immune microenvironments among differentially growing metastases in an ovarian cancer patient. *Cell*. 2017;170:927-938.e20.
39. Navin N, Kendall J, Troge J, et al. Tumour evolution inferred by single-cell sequencing. *Nature*. 2011;472:90-94.
40. Zhang J, Fujimoto J, Wedge DC, et al. Intratumor heterogeneity in localized lung adenocarcinomas delineated by multiregion sequencing. *Science*. 2014;346:256-259.
41. Zehir A, Benayed R, Shah RH, et al. Mutational landscape of metastatic cancer revealed from prospective clinical sequencing of 10,000 patients. *Nat Med*. 2017;23:703-713.
42. Murakami R, Matsumura N, Brown JB, et al. Exome sequencing landscape analysis in ovarian clear cell carcinoma shed light on key chromosomal regions and mutation gene networks. *Am J Pathol*. 2017;187:2246-2258.
43. Rathinaswamy MK, Burke JE. Class I phosphoinositide 3-kinase (PI3K) regulatory subunits and their roles in signaling and disease. *Adv Biol Regul*. 2020;75:100657.
44. D'Ambrosio C, Erriquez J, Arigoni M, et al. PIK3R1W624R is an actionable mutation in high grade serous ovarian carcinoma. *Cell*. 2020;9:442.
45. Deng J, Bai X, Feng X, et al. Inhibition of PI3K/Akt/mTOR signaling pathway alleviates ovarian cancer chemoresistance through reversing epithelial-mesenchymal transition and decreasing cancer stem cell marker expression. *BMC Cancer*. 2019;19:618.
46. Kinross KM, Montgomery KG, Kleinschmidt M, et al. An activating Pik3ca mutation coupled with Pten loss is sufficient to initiate ovarian tumorigenesis in mice. *J Clin Invest*. 2012;122:553-557.
47. Westfall SD, Skinner MK. Inhibition of phosphatidylinositol 3-kinase sensitizes ovarian cancer cells to carboplatin and allows adjunct chemotherapy treatment. *Mol Cancer Ther*. 2005;4:1764-1771.
48. Choi HJ, Heo JH, Park JY, et al. A novel PI3K/mTOR dual inhibitor, CMG002, overcomes the chemoresistance in ovarian cancer. *Gynecol Oncol*. 2019;153:135-148.

SUPPORTING INFORMATION

Additional supporting information may be found in the online version of the article at the publisher's website.

How to cite this article: Lupia M, Melocchi V, Bizzaro F, et al. Integrated molecular profiling of patient-derived ovarian cancer models identifies clinically relevant signatures and tumor vulnerabilities. *Int. J. Cancer*. 2022;1-15. doi:10.1002/ijc.33983